Motor protein KIFC5A interacts with Nubp1 and Nubp2, and is implicated in the regulation of centrosome duplication

Andri Christodoulou[1], Carsten W. Lederer[1], Thomas Surrey[2], Isabelle Vernos[2,*] and Niovi Santama[1,‡]

[1]Department of Biological Sciences, University of Cyprus and Cyprus Institute of Neurology and Genetics, PO Box 20537, 1678 Nicosia, Cyprus
[2]Cell Biology and Biophysics Programme, European Molecular Biology Laboratory, Meyerhofstrasse 1, 69117 Heidelberg, Germany
*Present address: Cell and Developmental Biology Program, CRG, Centre de Regulació Genòmica, Passeig Marítim 37-49, 08003 Barcelona, Spain
‡Author for correspondence (e-mail: santama@ucy.ac.cy)

Accepted 3 February 2006
Journal of Cell Science 119, 2035-2047 Published by The Company of Biologists 2006
doi:10.1242/jcs.02922

Summary

Inhibition of motor protein activity has been linked with defects in the formation of poles in the spindle of dividing cells. However, the molecular mechanisms underlying the functional relationship between motor activity and centrosome dynamics have remained uncharacterised. Here, we characterise KIFC5A, a mouse kinesin-like protein that is highly expressed in dividing cells and tissues, and is subject to developmental and cell-type-specific regulation. KIFC5A is a minus-end-directed, microtubule-dependent motor that produces velocities of up to 1.26 μm minute^{-1} in gliding assays and possesses microtubule bundling activity. It is nuclear in interphase, localises to the centre of the two microtubule asters at the beginning of mitosis, and to spindle microtubules in later mitotic phases. Overexpression of KIFC5A in mouse cells causes the formation of aberrant, non-separated microtubule asters and mitotic arrest in a prometaphase-like state. KIFC5A knockdown partly rescues the phenotype caused by inhibition of plus-end-directed motor Eg5 by monastrol on the mitotic spindle, indicating that it is involved in the balance of forces determining bipolar spindle assembly and integrity. Silencing of KIFC5A also results in centrosome amplification detectable throughout the cell cycle. Supernumerary centrosomes arise primarily as a result of reduplication and partly as a result of cytokinesis defects. They contain duplicated centrioles and have the ability to organise microtubule asters, resulting in the formation of multipolar spindles. We show that KIFC5A interacts with nucleotide-binding proteins 1 and 2 (Nubp1 and Nubp2), which have extensive sequence similarity to prokaryotic division-site-determining protein MinD. Nubp1 and Nubp2 also interact with each other. Knockdown of Nubp1 or double knockdown of Nubp1 and Nubp2 (Nubp1&Nubp2) both phenocopy the KIFC5A silencing effect. These results implicate KIFC5A and the Nubp proteins in a common regulatory pathway involved in the control of centrosome duplication in mammalian cells.

Supplementary material available online at
http://jcs.biologists.org/cgi/content/full/119/10/2035/DC1

Key words: Centrosome, Nubp1, Nubp2, Mitosis, Spindle

Introduction

The mitotic spindle is a complex microtubule (MT)-based bipolar structure, whose assembly, dynamic changes and disassembly follow a well-regulated choreography. This is largely driven by the coordinated activities of plus-end- and minus-end-directed motor proteins, the dynamic behaviour of MTs and local activity of chromosomes, the participation of structural proteins and the reversible effects of various enzymatic activities (Compton, 2000; Karsenti and Vernos, 2001).

Minus-end-directed kinesin-like proteins (KLPs) of the Kinesin-14 family (Lawrence et al., 2004), previously referred to as KINC (Ovechkina and Wordeman, 2003), are among the important players for spindle assembly and maintenance. Family members include protein isoforms from *Drosophila* (Ncd) (Walker et al., 1990; McDonald et al., 1990), hamster (CHO2) (Kuriyama et al., 1995; Matuliene et al., 1999), *Xenopus* (XCTK2) (Walczak et al., 1997), human (HSET) (Ando et al., 1994; Mountain et al., 1999), mouse (KIFC5A) (Navolanic and Sperry, 2000; Zhang and Sperry, 2004), and others. Although there are differences between species, Kinesin-14 motors, in general, localise to the centrosomes at spindle poles and, through their minus-end motility and ability to bundle MTs, are thought to be important for the formation of focused asters, the establishment of spindle bipolarity and the maintenance of spindle integrity (reviewed by Ovechkina and Wordeman, 2003).

Despite the wealth of information about particular members of the Kinesin-14 family, our understanding about their precise role in organising asters and maintaining spindle bipolarity remains sketchy, and the mechanisms and participants involved are not well characterised. At the same time, the centrosome, although not always essential for aster formation, is receiving renewed attention for its key role in controlling cell division, including initiation of cytokinesis and entry into S phase of the cell cycle (Piel et al., 2001; de Bettignies and Johnston, 2003), as well as its involvement in tumourigenesis and human genetic disease (Nigg, 2002; Saunders, 2005; Badano et al., 2005). The centrosome duplication cycle is regulated by a complex set of

cell-cycle-specific proteins (e.g. Cdk, Aurora/Ip11, Polo-like and NIMA families of kinases), tumour suppression proteins (e.g. p53, TACC and BRCA1) and structural proteins (e.g. NuMA) (reviewed by Ou and Rattner, 2004). The combined activities of these regulatory proteins underline the cell-cycle-specific compositional modifications of the centrosome and its specific interactions, which enable progression through the defined steps of its duplication cycle in coordination with DNA replication (Ou and Rattner, 2004). The possible contribution of motor proteins in the regulation of centrosome duplication remains uncharted. Although there are several examples of spindle pole formation defects by inhibition of motor protein activity [such as the comprehensive analysis by Goshima and Vale (Goshima and Vale, 2003)], suggesting a functional association between motor proteins and the centrosome cycle, the putative pathways of this association still remain unknown and uncharacterised. This shortcoming is rooted in our confined knowledge of other proteins involved and, in turn, limits our emerging molecular understanding of the regulatory circuits that govern centrosome dynamics in health and disease. As deregulation of the centrosome number has the potential to foster chromosomal instability in cancer cells (Nigg, 2002), elucidation of the regulatory mechanisms underlying centrosome duplication will thus increasingly attract attention as the basis for centrosome-related diagnostic or therapeutic approaches.

In this work, we wish to investigate KIFC5A, the murine mitotic motor of the Kinesin-14 family, understand in more depth its role in aster formation and in the definition of spindle bipolarity, address its functional association with the centrosome, and begin to unravel its possible functional contribution to the centrosome cycle. We detail the characterisation of KIFC5A, reveal its interactions with the novel mouse proteins Nubp1 and Nubp2, which share extensive sequence similarity with bacterial division-site-determining proteins, and show that KIFC5A is involved in the regulation of centrosome reduplication.

Results

Identification of KIFC5A from mouse hippocampus

KLPs that are developmentally regulated during neuronal differentiation in mouse hippocampus were identified by a degenerate PCR-based approach (see Santama, 2001), using cDNA pools isolated from hippocampi of distinct developmental stages in mouse. One partial cDNA, enriched in the hippocampus of embryonic stage E13, was identified as that corresponding to KIFC5A, the murine homologue of Kinesin-14 family members. The full-length open reading frame (ORF) of KIFC5A was amplified from E13 hippocampal cDNA using sequence-specific oligos (Fig. 1, EMBL accession no. AM051187). The ORF is predicted from the cDNA sequence to encode a 631 amino acid (aa) protein (Fig. 1A), and includes a conserved KLP motor domain (aa 300 to 631) at the C-terminus. Secondary structure and coiled-coil prediction indicate an α-helical coiled-coil stalk (aa 94 to 264, Fig. 1B) at the N-terminus. The expected M_r of the 631 aa peptide is 69.253×10^3. Consistently, a unique band of the appropriate size was detected by immunoblot analysis with an antibody raised to a non-conserved C-terminal peptide (Fig. 1C).

KIFC5A expression is cell-type-specific and developmentally regulated

To examine the expression profile of KIFC5A in the mouse hippocampus, a semi-quantitative reverse transcriptase (RT)-PCR analysis was carried out using equivalent amounts of cDNA synthesised using isolated hippocampi of E13 and E18 mouse embryos, as well as hippocampi from juvenile and adult animals (Fig. 2). This showed that, whereas KIFC5A expression is abundant in the hippocampus at the early embryonic stage E13, it is markedly downregulated by E18 and is hardly detectable postnatally (Fig. 2A). Given that a proportion of glial cells are present in the hippocampal structure, and to distinguish possible differences between the main cell types of nervous tissue (neurons and glia), the

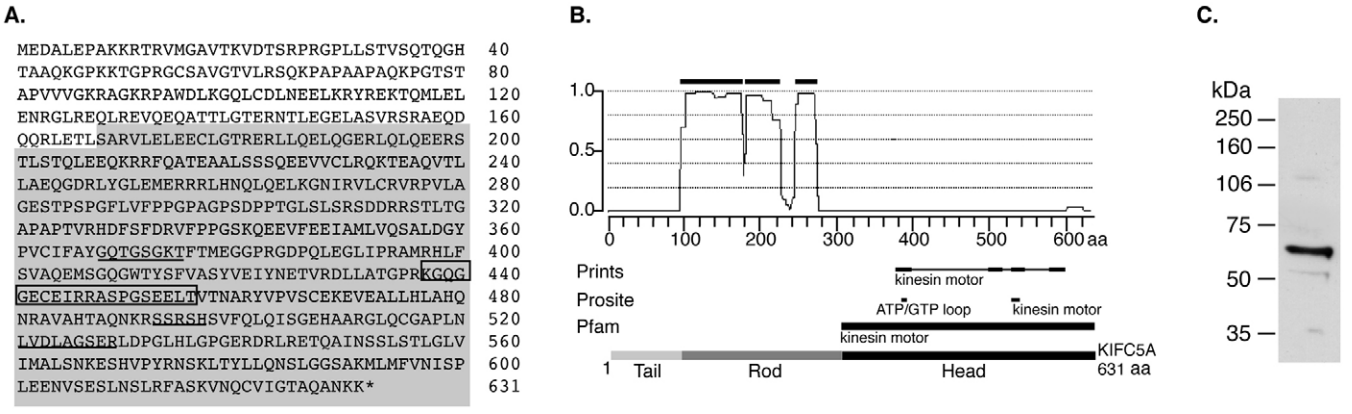

Fig. 1. (A) Deduced protein sequence of mouse KIFC5A, isolated from the hippocampus of embryonic stage E13. The motor domain is located at the C-terminal. Underlined sequences are conserved motor domain 'signature motifs', including the ATP-binding site (GX_4GKT). The sequence to which an anti-peptide antiserum was produced is boxed. Shading shows the sequence of recombinant KIFC5A-s, used for motility and protein interaction assays. (B) Predicted probability of coiled-coil formation and protein domains in KIFC5A. Prediction of coils was based on the algorithm of Lupas et al. (Lupas et al., 1991) and domain analysis was performed using the Predict Protein Server (Rost and Liu, 2003). A sketch of KIFC5A overall organisation is shown at the bottom of the panel. (C) Detection of KIFC5A in NIH 3T3 cells. Western blot analysis of a total protein extract from NIH 3T3 fibroblasts, using the affinity-purified anti-peptide antibody to KIFC5A, reveals a band consistent with the predicted M_r of 69.253×10^3.

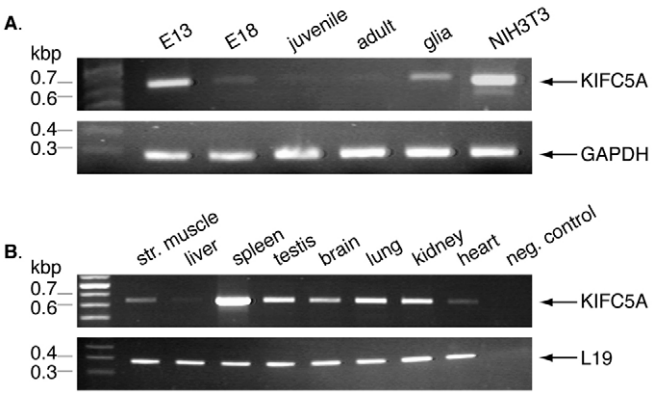

Fig. 2. Expression of KIFC5A in the brain is subject to developmental and cell-type-specific regulation. (A) Comparative analysis of levels of KIFC5A cDNA (oligo set 3), synthesised from identical amounts of RNA isolated from the hippocampus of E13 and E18 mice, juvenile (2.5 weeks) and adult (3 months) animals, as well as from pure, proliferating, glia astrocyte cultures (newborn animals) and NIH 3T3 fibroblasts. Equivalent reactions for GAPDH (oligo set 4) were used as internal standards (bottom panel). (B) Tissue-specific pattern of expression of KIFC5A. Equivalent RT-PCR reactions from various mouse tissues (Str., striated). A mock reverse transcription reaction with E13 RNA was the negative (neg.) control. Equivalent reactions for L19 (oligo set 5) were used as internal standards (bottom panel).

analysis extended to a pure astrocytic primary culture. In this material, abundant expression of KIFC5A was detected (Fig. 2A). In addition, the NIH 3T3 mouse fibroblast line displayed the highest relative expression of KIFC5A (Fig. 2A). An analysis of several mouse tissues showed that, whereas expression of KIFC5A is widespread, it is more pronounced in tissues that contain a higher proportion of actively dividing cells (spleen, testis, lung, kidney) and is significantly lower in tissues that are mainly post-mitotic (striated muscle, liver, heart and brain) (Fig. 2B). Taken together, these results indicate high expression of KIFC5A associated with developmental stages or cell types that are actively dividing, with little or no expression in tissues that contain few or no mitotic cells.

KIFC5A is a minus-end motor with a distinct spindle localisation

For the biophysical characterisation of KIFC5A, a truncated construct (KIFC5A-s) comprising an N-terminal His_6 tag, part of the N-terminal coiled-coil region of KIFC5A (from aa 168) and the entire motor domain (Fig. 1A) was expressed in *Escherichia coli* and affinity purified. Recombinant KIFC5A-s displayed a MT-stimulated ATPase activity of 1.65 molecules of ATP per second in the presence of 4 μM MTs (data not shown). KIFC5A-s, pre-bound with an anti-His_6-specific antibody and attached to a glass surface, could translocate taxol-stabilised MTs at a velocity of up to 1.26 μm minute^{-1}, n=40 (95% confidence) (Fig. 3A). Polarity-marked MTs moved with their plus-end leading, indicating that KIFC5A is a minus-end-directed motor protein (Fig. 3B). We noticed that, like other C-terminal motors (Walczak et al., 1997; Karabay and Walker, 1999), KIFC5A had the tendency to bundle MTs when mixed in solution.

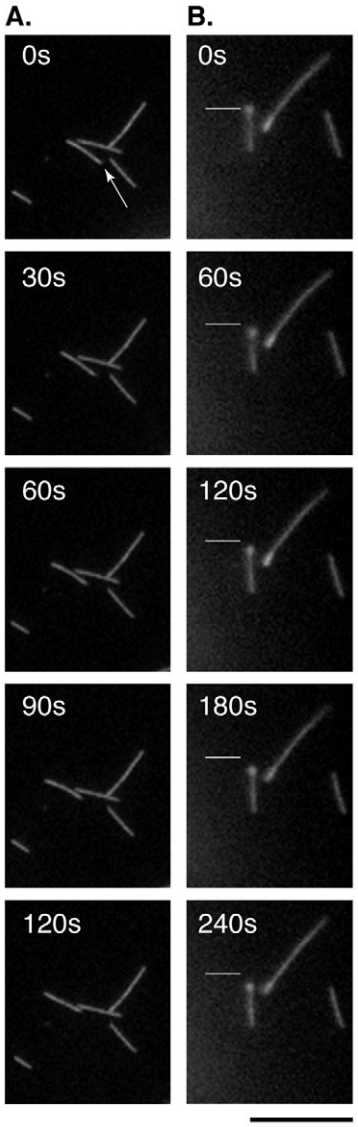

Fig. 3. (A) In vitro motility assay of fluorescently labelled MTs in the presence of the affinity-purified recombinant truncated protein KIFC5A-s. Movement of MTs on coverslips coated with KIFC5A-s was studied. The arrow points to a gliding MT. MTs moved at a maximum speed of 1.26 μm minute^{-1}, n=40 (95% confidence). (B) Movement of polarity-marked MTs on recombinant KIFC5A-s. The minus-end of MTs is more brightly labelled. The white bar is at a stable position in all panels. The MT shown glided towards its plus-end, indicating minus-end-directed motility of KIFC5A. Video images were taken at the indicated time intervals (s, seconds). Bar, 10 μm.

We next analysed the intracellular localisation of KIFC5A in NIH 3T3 mouse fibroblasts using an affinity-purified anti-peptide antibody to KIFC5A that recognises a unique band of the expected size for KIFC5A in NIH 3T3 extracts (Fig. 1C). The immunofluorescence analysis (Fig. 4A) revealed that, in interphase cells, KIFC5A displayed an exclusively nuclear localisation, excluding nucleoli. Throughout mitosis, KIFC5A labelling was confined to the mitotic spindle with distinct localisations in the different mitotic phases (Fig. 4A). In prophase, KIFC5A was heavily concentrated at the centre of the two separating microtubule asters. From prometaphase through to anaphase, KIFC5A labelling covered most spindle MTs (Fig. 4A). In telophase, KIFC5A was again confined to the reformed daughter nuclei and the midbody constriction (not shown).

The intracellular localisation of KIFC5A throughout the cell cycle was also followed by transient transfection of a yellow fluorescent protein (YFP)-tagged KIFC5A construct in NIH 3T3 cells (Fig. 4B). The results obtained (Fig. 4B), as well as results from parallel experiments using a myc-tagged version of KIFC5A for transfections (data not shown), were identical

to those observed by immunofluorescence with the anti-KIFC5A antibody (Fig. 4A).

KIFC5A activity during mitosis is crucial for correct aster formation and for spindle assembly

The complex process of spindle formation and its dynamics are in part the result of a delicate balance of opposing motor forces. To elucidate in greater depth the specific role of the mitotic motor KIFC5A in this context, we conducted functional experiments in which the expression of KIFC5A was either significantly increased or reduced, and assessed the effects of these manipulations on spindle assembly and integrity.

Transient transfections of NIH 3T3 with YFP-KIFC5A were carried out, resulting in high-level expression of intact YFP-KIFC5A in these cells (immunoblot data not shown). Control transfections with the YFP-alone vector were performed in parallel. Cells were processed for triple fluorescence to visualise YFP-KIFC5A, MTs and DNA. A high proportion of mitotic YFP-KIFC5A-overexpressing cells (56%) displayed a strikingly altered spindle morphology and arrested in a prometaphase-like stage (Fig. 5), compared with the control group (only 2.66%) (Table 1). This difference was statistically significant (P=1.67×10^{-4}). Later stages of mitosis (metaphase and anaphase) were rarely observed in YFP-KIFC5A-expressing cells (4.88% of mitotic cells) whereas, in the control cells, they accounted for 12% of the mitotic figures (Table 1). In addition, whereas 72% of mitotic cells in the control group were in telophase, less than half of this proportion of mitotic cells (34.15%) in overexpressing cultures was counted in telophase (Table 1). The combination of these findings indicated that overexpression of YFP-KIFC5A in mitotic cells induced stalling of mitotic progression in prometaphase. The decreased overall percentage of mitotic overexpressing cells (1.9% versus 3.7% in controls) could also suggest an increased rate of apoptosis, possibly as a result of a prolonged block in prometaphase. In conclusion, the overall distribution of cells in distinct phases of mitosis was significantly different in overexpressing and control samples (P=2.11×10^{-10}).

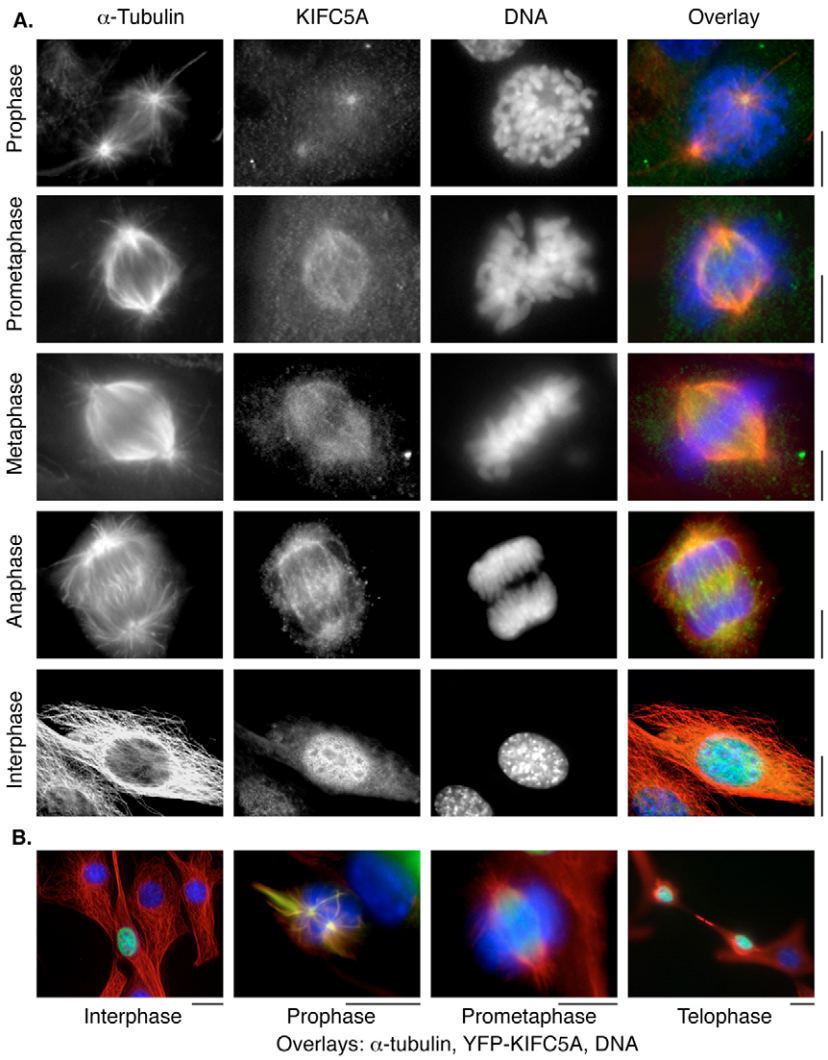

Fig. 4. Localisation of KIFC5A during the phases of the cell cycle in NIH 3T3 fibroblasts. (A) NIH 3T3 cells were processed for immunofluorescence with an antibody against α-tubulin (red) and an antibody against KIFC5A (green). DNA was visualised with Hoechst (blue). (See also Fig. S4, supplementary material.) Bars, 5 μm. (B) NIH 3T3 cells, transiently transfected with YFP-KIFC5A. Only overlays are shown, with α-tubulin staining in red, YFP-KIFC5A in green and DNA in blue. In the left-most panel, visualising a field of cells in interphase, only one cell is transfected. YFP-KIFC5A localisation matches closely that of the endogenous KIFC5A (panels in A). Bars, 10 μm.

Closer microscopic analysis of the YFP-KIFC5A-overexpressing cells arrested in a prometaphase-like state revealed the presence of microtubule asters that appeared non-separated, remained either at very close distance to each other (Fig. 5A top row) or even fused, forming a single microtubule aster (Fig. 5A bottom row). This phenotype was identical in cells overexpressing myc-KIFC5A fusions (Fig. 5A bottom row) and therefore was independent of the tag used.

Double labelling with an anti-pericentrin antibody confirmed the presence of the two centrosomes at the centre of the non-separated asters (Fig. 5B top row, compare with bottom row). MTs that appeared bundled emanated radially from the non-separated centrosomes, and condensed chromatin was positioned at the centre of the aster close to the centrosomes (Fig. 5A,B). The bundling of MTs in these figures was consistent with the bundling of MTs by recombinant KIFC5A-s in vitro. The quantitative results (Table 1) and morphological analysis (Fig. 5) indicate that overexpression of KIFC5A interferes with bipolar spindle formation, most probably by blocking centrosome separation or, alternatively, by causing spindle collapse, or both. As a consequence, mitotic cells remain stalled or delayed at prometaphase and unable to proceed to subsequent phases and successfully complete mitosis.

Table 1. Effect of KIFC5A overexpression in NIH 3T3 cells

	Control transfection (YFP-alone vector)	YFP-KIFC5A transfection
Transfected cells counted	2001	2205
Number of cells in mitosis		
of which:	75 (3.7% of total)	41 (1.9% of total)
normal prophase/ prometaphase	10 (13.3% of mitotic)	2 (4.88% of mitotic)
stalled prometaphase*	2 (2.7% of mitotic)	23 (56% of mitotic)
metaphase	3 (4% of mitotic)	1 (2.4% of mitotic)
anaphase	6 (8% of mitotic)	1 (2.4% of mitotic)
telophase	54 (72% of mitotic)	14 (34.1% of mitotic)

*See Fig. 5.

The percentage of cells in stalled prometaphase in YFP-KIFC5A-expressing cells is significantly different than in the control population (single-factor ANOVA with replication, $P=1.67\times10^{-4}$). The overall distribution of cells in distinct phases of mitosis is significantly different in overexpressing and control samples (multiple-factor ANOVA with replication, $P=2.11\times10^{-10}$).

Table 2. Effect of KIFC5A silencing on the number of centrosomes in mitotic cells

siRNA		Control	KIFC5A
Number of mitotic cells counted		802	209
Cells with	2 centrosomes	678 (84.5%)	83 (39.7%)
	3 centrosomes	78 (9.7%)	52 (24.9%)
	4 centrosomes	33 (4.1%)	26 (12.4%)
	5 centrosomes	6 (0.7%)	18 (8.6%)
	6 centrosomes	3 (0.4%)	14 (6.7%)
	7 centrosomes	2 (0.2%)	7 (3.3%)
	8 centrosomes	–	4 (1.9%)
	9 centrosomes	2 (0.2%)	2 (1%)
	⩾10 centrosomes	–	3 (1.4%)
Cells with multiple centrosomes (% total)		124 (15.5%)	126 (60.3%)
Average number of centrosomes per cell (% of mitotic cells counted)		2.25	3.49

The average number of centrosomes is significantly higher between silencing and control treatment (single-factor ANOVA with replication, $P=0.006$).

Reduction of KIFC5A expression induces centrosome amplification primarily by reduplication

To assess the effect of the reduction of KIFC5A expression on spindle assembly, we employed RNA interference and obtained a specific reduction in both KIFC5A mRNA and protein levels at 120 hours post-transfection (Fig. 6A1,A2). An average knockdown of KIFC5A mRNA to 27±10.5% of control short interfering (si)RNA-treated levels (Fig. 6A1), and a reduction of protein levels to approximately 35% of control-silenced cells (Fig. 6A2), was achieved. Furthermore, in KIFC5A-silenced cells, KIFC5A was barely detectable by immunofluorescence (compare Fig. 6A3 top and bottom row at identical exposure of 300 milliseconds).

Microscopic examination of KIFC5A-silenced cells revealed the presence of a markedly increased number of centrosomes in mitosis (initially identified as γ-tubulin-positive foci) and the formation of anomalous multi-polar spindles in mitotic cells (Fig. 6B2). Quantification of these phenotypes showed that, following KIFC5A silencing, the percentage of mitotic cells with two centrosomes was reduced to half the value found in control cells (39.7% versus 84.5%) and the percentage of mitotic cells with multiple centrosomes was four times higher than in control cells (60.3% versus 15.5%) (Fig. 6B1 and Table 2). The average number of centrosomes per cell had changed significantly from 2.25 for control-silenced cells to 3.49 following KIFC5A silencing ($P=0.006$) (Table 2).

To ascertain that the γ-tubulin-positive foci corresponded to bona fide centrosomes, silenced cells were double labelled with an anti-centrin antibody (as a centriolar marker) in conjunction with anti-γ-tubulin. These experiments revealed an exact correspondence between centrin-positive and γ-tubulin-positive foci (Fig. 6B2). Furthermore, quantification of the silencing phenotype by scoring the number of centrosomes with the use of centrin as a marker (data not shown) gave comparable results to those presented in Fig. 6B1 and Table 2, using γ-tubulin as a marker. We next addressed the state of

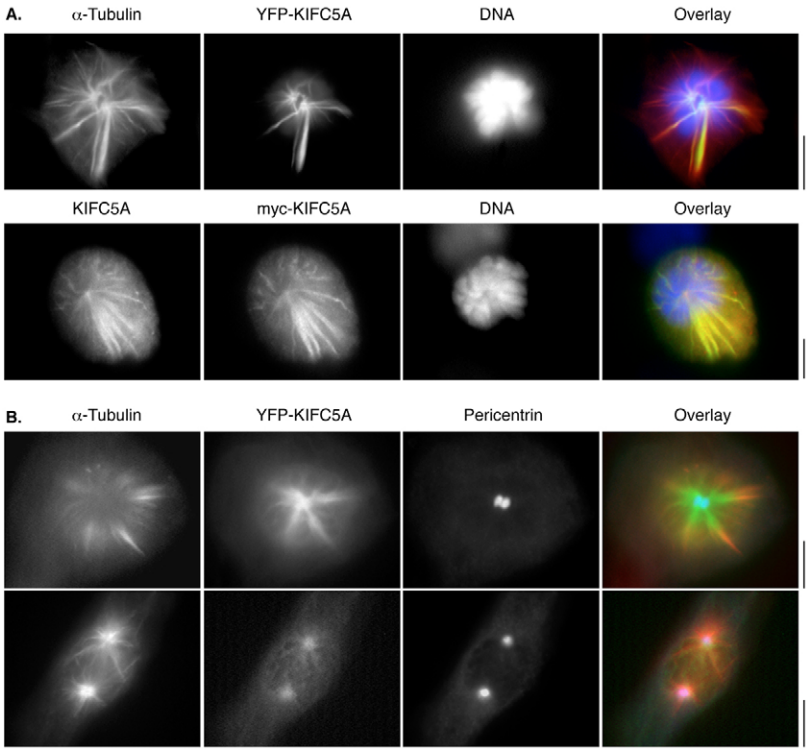

Fig. 5. Overexpression of KIFC5A inhibits bipolar spindle formation and causes stalling of mitotic progression in prometaphase. (A) Two typical examples of NIH 3T3 cells overexpressing YFP-KIFC5A (top panel) or myc-KIFC5A (bottom panel). Cells were labelled for α-tubulin (red) or myc (green). DNA was visualised with Hoechst (blue), YFP-KIFC5A is green. Bars, 5 μm. (B) Another example of the 'stalled phenotype' in prometaphase with the use of anti-pericentrin (top panel). In the overlay, YFP-KIFC5A is green, α-tubulin staining is red and pericentrin is blue. A normal cell in prometaphase is shown for comparison (bottom panel). Bars, 5 μm.

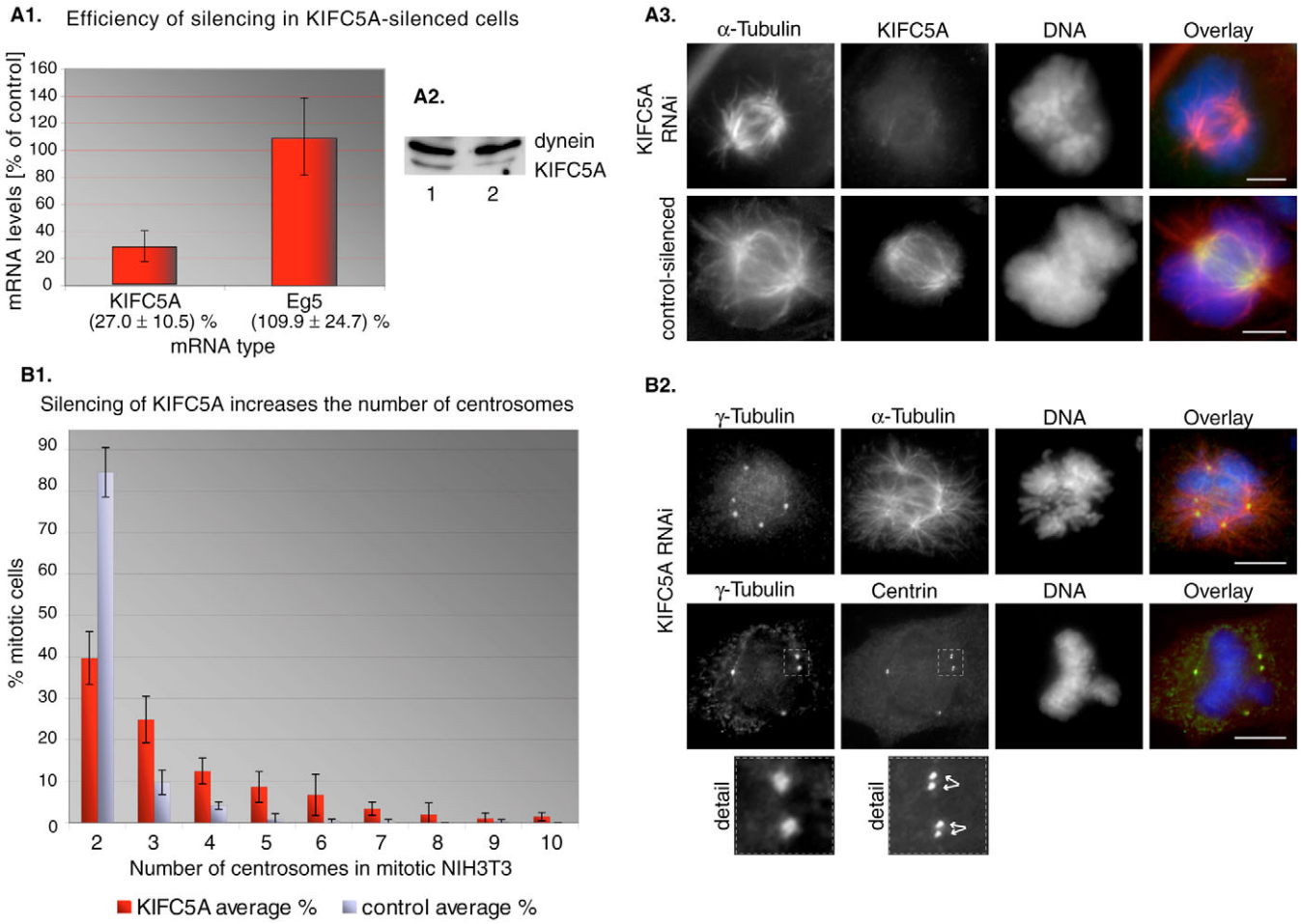

Fig. 6. RNAi-mediated silencing of KIFC5A causes centrosome amplification and aberrant multi-polar spindles in NIH 3T3 cells. (A1) Efficiency of silencing by quantitative real-time PCR. This shows an average knockdown of KIFC5A mRNA to 27.0±10.5% (s.d.) of control-silenced levels (silencing with medium GC content control silencing oligo; see Materials and Methods), whereas mRNA of the (unrelated) mitotic motor protein Eg5 shows 109.9±24.7% of control on average. mRNA levels of the *PBGD* housekeeping gene were used for sample normalisation. (A2) Efficiency of silencing by western blot. This shows a visible reduction of KIFC5A protein levels in silenced cells (lane 2; approx. 35%), compared with control-silenced cells (lane 1). Dynein detection (upper band) served as an internal loading control. (A3) Verification of silencing by triple immunofluorescence. Cells were immunolabelled for α-tubulin, KIFC5A and counterstained for DNA (red, green and blue in the overlay, respectively). Whereas the lower panels (control-silenced cell) show normal KIFC5A labelling of the spindle in prometaphase, labelling is hardly detectable in the KIFC5A-silenced cell (upper panels) at the same exposure (300 milliseconds). Bars, 5 μm. (B1) Quantification of the silencing effect on centrosome numbers in mitotic cells. KIFC5A-silenced mitotic cells contain a higher number of centrosomes per cell, 120 hours after initial siRNA treatment, compared with the control. Shown are the means from three independent experiments (see also Table 2). Bars represent s.d. values. (B2) Immunofluorescence of silenced cells, displaying an increase in the number of centrosomes and spindle poles. The top panel shows an example of a KIFC5A-silenced cell, immunostained for γ-tubulin (green), α-tubulin (red) and counterstained for DNA (blue). In the bottom panel, anti-centrin, instead of α-tubulin, was used. The exact match between γ-tubulin (green) and centrin (red) labelling can be observed. The extracted detail in insets (bottom) illustrates that supernumerary centrosomes consist of duplicated centrioles (arrows). Bars, 10 μm.

duplication for these centrosomes by determining the number of centrioles each contained. Close microscopic examination (Fig. 6B2, detail in insets) indicated that most of these centrosomes, forming multipolar spindles, contained duplicated centrioles [89.81% of centrosomes contained two centrioles and 10.19% had only one centriole, n=50 cells. This percentage of unicentriolar centrosomes was close to control-silenced levels (12.10%)].

We next examined whether centrosome amplification extended beyond mitosis by counting centrin-positive and γ-tubulin-positive centrosomes in interphase cells. This revealed that the average number of centrosomes per cell in KIFC5A-silenced interphase cells was also statistically significantly higher than in control-silenced cells (2.68 versus 2.19, P=0.020; Table S1, supplementary material). To investigate whether the existence of multiple centrosomes and spindle poles in silenced cells affected normal progression through the cell cycle, two experimental lines of investigation were pursued. The cell-cycle profile of populations of silenced and control cultures was determined both by fluorescence activated cell sorter (FACS) analysis and by microscopic examination of large numbers of cells (>10^5). Both FACS analysis (Table 3) and microscopic evaluation (Table S2, supplementary material) showed a statistically significant difference of the mitotic index

Table 3. FACS analysis of KIFC5A-silenced and control-silenced cells

Cell-cycle phase	siRNA control	KIFC5A siRNA
G0-G1	76.19%	65.94%
S	16.96%	24.62%
G2-M	6.85%	9.43%
Total cells counted	19,171	20,699

(P=0.015). In particular, there was an increase in the number of cells in S phase in the KIFC5A-silenced cells compared with the control-silenced culture (Table 3). Furthermore, there is a near doubling of the mitotic index in KIFC5A-silenced cells (1.13% of cells are in mitosis) versus control-silenced cells (0.58%) (Table S2, supplementary material). These findings appear consistent with the observed amplification of duplicated centrosomes in mitosis.

Finally, in KIFC5A-silenced cells, we also observed a statistically significant increase (P=0.0018) in the number of cells having more than one nucleus (17.91%, Table S3, supplementary material), suggesting cytokinesis failure (binucleated cells reached 13.62% of the total number of cells whereas only 0.97% were observed in control-silenced cells). It is noteworthy that supernumerary centrosomes were present in both mononucleated cells (representing >60% of cells with supernumerary centrosomes) and multinucleated cells alike. This finding suggested that defects in cytokinesis might not be the main mechanism involved in centrosome amplification, although it could contribute to it.

Silencing of KIFC5A partly relieves the effect of Eg5 inhibitor monastrol on the mitotic spindle

To better characterise the concerted action of KIFC5A with other mitotic motors that are known to participate in spindle assembly, we examined the consequences of inhibiting the mitotic motor Eg5 with monastrol at the same time as silencing KIFC5A. Given that Eg5 is a plus-end-directed mitotic motor essential for the establishment and maintenance of spindle bipolarity, we investigated whether the absence of minus-end-directed activity of KIFC5A could alleviate the distinct and well-characterised phenotype caused by the inhibition of Eg5 (Kapoor et al., 2000) by restoring the balance of opposing motor forces in the forming spindle.

Treatment of control-silenced cells with monastrol resulted in 93.5% of all mitotic cells (>10^5 cells counted) exhibiting the typical Eg5 inhibition phenotype, consisting of a single radial microtubule array with chromosomes forming a cartwheel structure. Only 6.5% of cells in various mitotic phases possessed a normal phenotype (Table S4, supplementary material). A combination of monastrol treatment and silencing of KIFC5A increased the percentage of mitotic cells with an apparent normal morphology by a factor of 4.8 to 31.4% (Table S4, supplementary material). These results strongly suggested a partial, but significant, rescue of the effects of Eg5 inhibition on the mitotic spindle by KIFC5A silencing. Interestingly, rescued cells displayed the typical phenotype of KIFC5A silencing with an increased average number of centrosomes per cell and multipolar spindles. In the same cultures, cells displaying the monastrol cartwheel phenotype frequently possessed multiple centrosomes that were clustered in the centre of the cartwheel formation.

KIFC5A interacts with Nubp1 and Nubp2, which share extensive sequence similarity to the MinD prokaryotic ATPase, a regulator of cell division

To probe further the mechanism through which KIFC5A might exert its function in spindle assembly, we sought to identify putative interacting partners for this motor using the yeast two-hybrid system. Of the 1.2 million clones of a mouse embryonic central nervous system cDNA library that were screened using KIFC5A-s as the bait (Fig. 7A), 36 positive clones were identified after several rounds of selection. Among these, two overlapping cDNAs, encoding the same ORF, were detected and the longest, an apparently full-length cDNA clone, was sequenced (Fig. 7B). A database search revealed that this positive clone corresponded to ‘nucleotide-binding protein 2’ (Nubp2, Fig. 7B), an ATPase of the NUBP/MRP subfamily (Nakashima et al., 1999). Mouse Nubp2 has extensive sequence similarity with prokaryotic protein MinD, a member of the NifH-ArsA-Par-MinD subgroup of type A ATPases (Walker et al., 1982; Koonin, 1993). In bacteria, MinD together with the *min* operon proteins MinC and MinE cooperatively determine the septation site for cell division (reviewed by Amos et al., 2004). Min proteins are organised in membrane-associated coils and undergo a rapid pole-to-pole oscillation movement in vivo (Shih et al., 2003; Raskin and de Boer, 1999). The important role of MinD in the accurate placement of the cell division machinery in prokaryotes (FtsZ ring), as well as its intriguing behaviour as a ‘motor protein in prokaryotes’ (Sakai et al., 2001), made the protein identified in our screen an attractive candidate for further study. Two mouse proteins with sequence similarity to MinD have been described so far: Nubp1 has a unique N-terminal extension containing four cysteine residues and Nubp2 is a shorter form without the N-terminal extension (Nakashima et al., 1999) (Fig. 7B). Nubp1 and Nubp2 are encoded by genes on different chromosomes and share a characteristic P-loop motif and two highly conserved NUBP/MRP motifs α and β (Nakashima et al., 1999) (Fig. 7B).

To ensure that the interaction detected was bona fide, we carried out an in vitro co-selection experiment. His_6-tagged KIFC5A-s, expressed in *E. coli*, was bound to Ni^{2+}-NTA beads and incubated with GFP-Nubp2 (Fig. 7C). This experiment showed that GFP-Nubp2 was recovered in the pellet fraction only when incubated in the presence of recombinant His_6-KIFC5A-s (as indicated by a band with the appropriate M_r of 52×10^3), consistent with an interaction between the two proteins (Fig. 7C, compare lane 1 with the negative controls in lanes 2 and 3). In the negative control lacking His_6-KIFC5A-s, no GFP-Nubp2 was recovered in the supernatant fraction (lanes 3 of the two blots) and His_6-KIFC5A-s did not bind non-specifically to GFP (lanes 2 of the two blots).

We next investigated the intracellular localisation of Nubp2 using an affinity-purified antibody raised against a unique peptide sequence in its C-terminus (Fig. 7B). The antibody specifically recognised a native protein of the appropriate size for Nubp2 in a lysate from NIH 3T3 cells (expected M_r 29.517×10^3, Fig. 7D). Immunofluorescent analysis of NIH 3T3 cells showed that Nubp2 appeared to concentrate mainly in the nucleus in interphase cells (Fig. 7E1). Throughout mitosis, Nubp2 labelling extended to the nucleocytoplasm surrounding the mitotic spindle, but was enriched at the poles of the mitotic spindle in prophase and prometaphase (Fig.

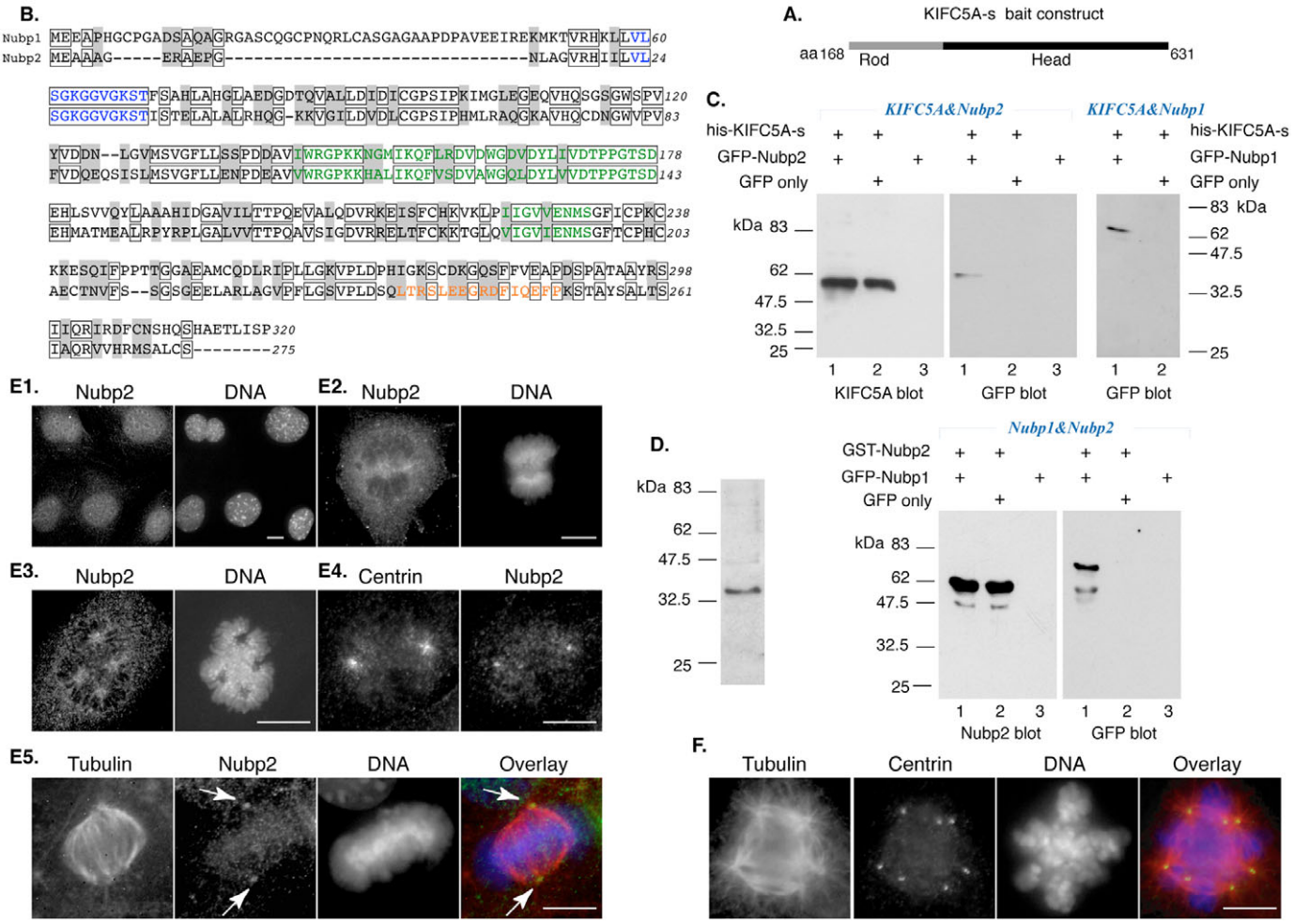

Fig. 7. (A) Diagram of the KIFC5A-s cDNA used as bait in the yeast two-hybrid system. (B) Protein sequence alignment between Nubp1 and Nubp2. Identical residues are boxed and conservative substitutions are highlighted in grey. The conserved ATP/GTP-binding motif (P loop) is marked in blue, the successive MRP motifs α and β are marked in green, and the sequence to which an anti-peptide serum to Nubp2 was produced is marked in orange. (C) In vitro co-selection experiments confirming interactions between KIFC5A&Nubp2, KIFC5A&Nubp1 and Nubp1&Nubp2. In the top panels, bacterially expressed tagged His_6-KIFC5A-s, immobilised on Ni^{2+}-NTA agarose beads, was incubated with a lysate from NIH 3T3 fibroblasts expressing GFP-Nubp2 or GFP-Nubp1 (lanes 1), or GFP only (negative control, lanes 2), or GFP-Nubp2 in the absence of pre-bound His_6-KIFC5A-s (additional negative control, lanes 3). Bound proteins were probed by immunoblotting with anti-KIFC5A (left panel) or anti-GFP (right panel). A positive signal (detection of GFP-Nubp2 or GFP-Nubp1) is obtained only in the presence of pre-bound His_6-KIFC5A-s (no signal in the absence of bound KIFC5A indicates that Nubp2 or Nubp1 does not bind the beads non-specifically). The co-selection of GFP-Nubp2 on the beads is not caused by interaction of KIFC5A with the FP domain (absence of signal in lane 2, right panel). In the bottom panels, the set-up of the experiment and negative controls is similar. GST-Nubp2 was immobilised on glutathione-Sepharose beads and was tested against GFP-Nubp1 (lanes 1), GFP only (negative control, lanes 2) or GFP-Nubp1 in the absence of GST-Nubp2 (additional negative control, lanes 3). Again, the positive signal (detection of Nubp1) was specific only in the presence of GST-Nubp2 (lanes 1). (D) Detection of native Nubp2 in NIH 3T3 cells. Western blot analysis of a total protein extract from NIH 3T3 fibroblasts, using the affinity-purified anti-peptide antibody to Nubp2, revealed a unique band consistent with the predicted M_r of Nubp2. (E) Localisation of Nubp2 in NIH 3T3 cells. Immunofluorescence for Nubp2 (green), centrin (red) and α-tubulin (red). DNA was visualised with Hoechst (blue). (E1) Cells in interphase; (E2) cell in prophase; (E3) an aberrant spindle with four asters in prometaphase; (E4) double labelling with anti-centrin and anti-Nubp2 in a cell in prometaphase; (E5) Nubp2 enrichment in centrosomes (arrows) of the fully formed metaphase spindle, shown by double labelling with α-tubulin. Bars, 10 μm (E2-E4) and 5 μm (E1). (F) Silencing phenotype after double Nubp1&Nubp2 RNAi, as revealed by triple fluorescence. Cells were immunolabelled for α-tubulin, centrin and counterstained for DNA (red, green and blue in the overlay, respectively). Bar, 10 μm.

7E2,E3). In later mitotic phases, Nubp2 immunofluorescence became more concentrated at the centrosomes. The localisation of Nubp2 in centrosomes was confirmed by double immunostaining with anti-centrin and anti-tubulin antibodies (Fig. 7E4,E5). Consistently, transient transfections with myc-tagged Nubp2 in NIH 3T3 fibroblasts also showed primarily nuclear accumulation of the protein in interphase and nucleocytoplasmic and spindle pole enrichment in mitosis, where Nubp2 co-localised with its interacting partner KIFC5A (data not shown).

To address the possible involvement of Nubp2 in spindle assembly, we tested the effect of Nubp2 downregulation by

RNA interference (RNAi) in NIH 3T3 cells. Expression of Nubp2 mRNA at 120 hours post-transfection showed a reduction to 8.6±5.9% of control-silenced levels (data not shown), indicating a satisfactory silencing effect. Microscopic assessment of the effects of Nubp2 reduction, using various markers for the mitotic spindle, did not reveal a discernible anomalous phenotype that was specifically associated with Nubp2-silenced cells. Furthermore, the cell-cycle profile was not statistically different between silencing and control treatment (data not shown).

Because of the lack of an apparent phenotype following Nubp2 knockdown, suggesting a possible redundancy in the mammalian system [in bacteria, MinD mutations cause the formation of 'mini cells' as a result of misregulated septation (de Boer et al., 1989)], we were prompted to examine the second MinD-like protein of eukaryotes, Nubp1. We first tested whether Nubp1 might also interact with KIFC5A and with Nubp2, using the yeast two-hybrid assay. These assays revealed specific interactions between KIFC5A&Nubp1 and Nubp1&Nubp2 (Fig. S1, supplementary material). Both sets of interactions were then confirmed by in vitro co-selection experiments, similar to those used for assaying the KIFC5A&Nubp2 interaction, including appropriate negative controls (Fig. 7C). We then assessed the effect of Nubp1 siRNA-mediated silencing. At 120 hours post-transfection, a specific reduction of Nubp1 mRNA to 26.53±10.33% of control-silenced cells was obtained. The phenotype of Nubp1-silenced cells was strikingly similar to that observed in KIFC5A-silenced cells, characterised by the same qualitative features: the presence of supernumerary centrosomes in cells at interphase and mitosis (resulting in the formation of multipolar spindles) and an increase in the proportion of bi- and tri-nucleated cells. Quantification of the results revealed that, in mitosis, there was a statistically significant increase of the average number of centrosomes per cell to 2.67, compared with 2.34 in control silenced cells (P=0.0035; Table 4). In interphase, the average number of centrosomes per cell increased significantly to 3.22, compared with 2.29 in control silenced cells (P=0.0048; Table S5, supplementary material). The proportion of multi-nucleated cells following Nubp1 silencing had increased significantly to 5.42%, compared with 2.08% of controls (P=6.15×10^{-6}) (Table S6, supplementary material). Taken together, these results indicated that, for comparable transcript knockdown efficiencies, Nubp1 silencing effects were qualitatively similar to those induced by KIFC5A silencing, but quantitatively 'milder'.

Finally, we tested the effects of simultaneous co-silencing of Nubp1&Nubp2 (Nubp1 mRNA was reduced to 14.74±1.53% and Nubp2 to 12.30±4.76%; Fig. S2, supplementary material); as quantitative controls, we tested in parallel single silencing with Nubp1, Nubp2 and control siRNAs. The co-silencing phenotype we observed (Fig. 7F) maintained the typical characteristics that were obtained with Nubp1-only silencing in a statistically significant manner, namely increase of the average number of centrosomes per cell in interphase (P=0.009, Table S7, supplementary material) and at mitosis (P=0.015, Table S8, supplementary material). Although there were small differences in both measurements in the combined Nubp1&Nubp2 silenced population compared with the corresponding values of Nubp1-only silencing carried out in parallel, none of those differences was statistically significant (Tables S7 and S8, supplementary material). An increase in the proportion of multi-nucleated cells was also maintained in Nubp1&Nubp2 silenced cells in a statistically significant manner compared with the control (P=0.0016, Table S9, supplementary material). Intriguingly, the values obtained with the double silencing for multiple nuclei were different from the corresponding values observed for Nubp1-only silencing in a statistically significant, albeit borderline, manner (P=0.046, Table S9, supplementary material). This could suggest a modulating role for Nubp2 affecting cytokinesis in concert with Nubp1 (Nubp2 silencing on its own has no effect on the number of nuclei per cell, P=0.222, Table S9, supplementary material).

Taken together, these findings show that KIFC5A interacts with both Nubps, which also interact with each other. The interactions and the resulting phenotypes indicate that KIFC5A with Nubp1 (and possibly Nubp2) are implicated in a common pathway controlling centrosome duplication.

Table 4. Effect of Nubp1 silencing on the number of centrosomes in mitotic cells

siRNA		Control	Nubp1
Number of mitotic cells counted		310	313
Cells with	2 centrosomes	268 (86.5%)	229 (73.2%)
	3 centrosomes	15 (4.8%)	35 (11.2%)
	4 centrosomes	13 (4.2%)	23 (7.3%)
	5 centrosomes	7 (2.3%)	6 (1.9%)
	6 centrosomes	–	10 (3.2%)
	7 centrosomes	4 (1.3%)	2 (0.6%)
	8 centrosomes	2 (0.6%)	6 (1.9%)
	9 centrosomes	–	–
	⩾10 centrosomes	1 (0.3%)	2 (0.6%)
Cells with multiple centrosomes (% total)		42 (13.5%)	84 (26.8%)
Average number of centrosomes per cell (% of mitotic cells counted)		2.34	2.67

The average number of centrosomes per cell is significantly higher between silencing and control treatment (single-factor ANOVA with replication, P=0.0035).

Discussion

In this work, we report the characterisation of mouse motor protein KIFC5A. KIFC5A belongs to the Kinesin-14 family and possesses a C-terminal motor domain. We show that it is abundant in tissues containing mitotic cells, primary dividing cells in culture (glial astrocytes), as well as cell lines. In mouse brain, it is highly expressed in early embryonic hippocampal tissue, is markedly downregulated in later developmental stages and is hardly detectable in the fully differentiated hippocampus of the adult. Although its presence in early developmental stages in the hippocampus could be attributed exclusively to glia, it is also plausible that KIFC5A expression at this stage might originate from neuronal precursors or early differentiating neurons.

Our in vitro motility assays confirmed that KIFC5A is a rather slow minus-end-directed motor with a velocity comparable with that of its homologues, yeast KAR3 (1-2 μm minute^{-1}) and hamster CHO2 (1.0-8.4 μm minute^{-1}), but slower than *Drosophila* Ncd (4-10 μm minute^{-1}). MT bundling observed in vitro as well as upon overexpression of KIFC5A in cells (see below) seems to be characteristic of Kinesin-14

family motors, where the existence of a second MT-binding site has been confirmed, at least for some members (Ncd) (Karabay and Walker, 1999).

Our in vivo results from both overexpression and RNA silencing clearly demonstrate that KIFC5A is one of the motors involved in spindle assembly. It also profoundly influences centrosome dynamics. Overexpression of KIFC5A in mouse fibroblasts causes defects in centrosome separation in early mitotic phases. This is consistent with findings for its homologues Ncd, XCTK2 and HSET, believed to contribute to spindle assembly by focusing MT minus-ends (Sharp et al., 1999; Walczak et al., 1997; Mountain et al., 1999). Alternatively, overexpression might disturb the maintenance of spindle bipolarity and cause spindle collapse as, for example, in Orbit/Mast-depleted cells (Inoue et al., 2000; Lemos et al., 2000; Maiato et al., 2002). A substantial body of research supports the view that spindle poles are sites of force integration. At least three motor activities – a Kinesin-14 family minus-end-directed motor, the plus-end-directed Eg5 and dynein-dynactin – are exerting antagonistic forces in establishing spindle bipolarity, in concert with non-motor proteins such as NuMA and TPX2 (Gaglio et al., 1996; Saunders et al., 1997; Mountain et al., 1999; Sharp et al., 1999; Garrett et al., 2002). A probable explanation for our overexpression phenotype is that the excess minus-end-directed force as a result of KIFC5A overexpression draws the two centrosomes close to each other, sliding along antiparallel MTs radiating from them, in line with prevailing models (Saunders and Hoyt, 1992). Compton and co-workers (Mountain et al., 1999) have provided an alternative model for the antagonistic forces of HSET and Eg5 acting to maintain centrosome separation later in mitosis in mammalian cells, based on their crosslinking activities and forces generated on parallel MT arrays. These ‘balance of forces’ models would predict that centrosome separation can be restored in the absence of the plus-end-directed Eg5 activity by concurrently reducing or eliminating the activity of the minus-end-directed motor (Saunders and Hoyt, 1992; Goshima and Vale, 2003; Miyamoto et al., 2004; Mitchison et al., 2005). This prediction was indeed confirmed by our experiments, which showed a partial rescue of the monastrol-induced inhibition of Eg5 through knockdown of KIFC5A.

Our most interesting novel finding was the profound effect on the centrosome cycle upon downregulation of KIFC5A by RNAi in mammalian somatic cells. Reduction of KIFC5A expression caused a significant centrosome amplification observed both at mitosis and at interphase. Supernumerary centrosomes appeared to be functional, as judged by the presence of duplicated centrioles and by their ability to focus MT asters and eventually organise multipolar spindles. The acquisition of additional centrosomes appeared as a gradual process requiring about 120 hours after siRNA application (corresponding to about five duplications of cells in culture) to observe its full impact. Although centrosome reduplications have been observed upon silencing of (the KIFC5A homologue) Ncd in the *Drosophila* S2 cell line (Goshima and Vale, 2003), the functional inhibition of (its human homologue) HSET by antibody injection of HeLa cells for the duration of one cell cycle (Mountain et al., 1999) did not yield the same phenotype, in line with this conclusion. All the evidence, therefore, points to a build-up mechanism linked to the cell cycle. Cells typically undergo only one round of centrosome duplication at S phase, in co-ordination with DNA synthesis. Pre-centriole formation occurs at the G1-S boundary. Each of the two centrioles duplicates at S phase in a semi-conservative manner, matures fully by G2-prophase, segregates to a daughter cell at cytokinesis and becomes licensed to undergo a novel round of duplication in the next cell cycle (reviewed by Ou and Rattner, 2004). The canonical cycle can be overridden by one of three mechanisms allowing centrosome overamplification (reviewed by Delattre and Gönczy, 2004): (1) by uncoupling centrosome duplication from DNA replication (Nigg, 2002; Saunders, 2005), (2) by aberrant splitting of centrosomes (Di Fiore et al., 2003) and (3) by a de novo centriole-assembly pathway at S phase (La Terra et al., 2005).

In our work, supernumerary centrosomes contain duplicated centrioles and persist in interphase, when mitotic unicentriolar centrosomes normally fuse, excluding aberrant splitting as an explanation for their formation. Defects in cytokinesis, as result of KIFC5A silencing, seem to contribute to centrosome accumulation to some extent. However, because the majority of cells containing supernumerary centrosomes are mononucleated (over 60%), it is clear that defects in cytokinesis are not the primary mechanism for centrosome accumulation. We cannot readily exclude mechanisms 1 or 3 as possible explanations for the acquisition of supernumerary centrosomes as a result of KIFC5A silencing, although these mechanisms are usually associated with particular physiological or experimentally induced conditions. The characteristics of the phenotype that we observe (i.e. apparent dependence of centrosome accumulation on cell duplication, presence of duplicated centrioles in supernumerary centrosomes) might, instead, suggest a leakage in the regulatory mechanism that governs licensing for centrosome duplication. This could cause the relaxation of the strict definition of one centrosome duplication per cell cycle and result in the gradual accumulation of supernumerary centrosomes upon multiple cell divisions. Although the licensing mechanism itself is not well characterised, a robust body of evidence shows that both pericentriolar material and the centriole undergo a compositional modification during the cell cycle (Ou and Rattner, 2004). The recruitment and/or loss of proteins can give rise to unique interactions specifying centrosome and spindle pole function during cell division. Intriguingly, the cargoes of KIFC5A are still unknown, and our results suggest that this motor protein might be involved in the recruitment (or sequestering) of crucial protein components that impose the centrosome reduplication block or, inversely, activate the licensing mechanism. The corresponding loss of fidelity in the licensing mechanism for centrosome reduplication, owing to significant KIFC5A reduction, would generate progressively more centrosomes with each cell division.

Despite the observed defects in cytokinesis, the presence of supernumerary centrosomes seems to be relatively well tolerated in NIH 3T3 cells. The percentage of apoptotic cells in silenced populations was moderate and comparable with controls, indicating that a large proportion of cells with multiple centrosomes, forming multipolar spindles, managed to undergo several cell cycles successfully. It is known that the presence of supernumerary centrosomes does not engage the

spindle assembly check point and allows correct attachment of kinetochores to spindle MTs (Sluder et al., 1997). In addition, cells utilise compensatory mechanisms, such as centrosome coalescence, in multipolar spindles and these functionally reduce the consequences of centrosome amplification so that some accuracy of chromosome segregation on a multipolar spindle is maintained (Sluder and Nordberg, 2004). We have indeed observed centrosome clustering in multipolar spindles (anti-diametrical alignment of multiple poles on spindles; Fig. S3, supplementary material), which could rely on MT-bundling forces (Sluder and Nordberg, 2004).

In our attempt to start unravelling the pathway through which KIFC5A activity exerts its effects on the regulation of centrosome duplication, we have identified Nubp1 and Nubp2 as proteins interacting with KIFC5A and with each other. We find that, in mammalian cells, Nubp2 is enriched in centrosomes in mitosis. Silencing experiments with Nubp2 did not give a discernible phenotype. However, knockdown of Nubp1 or double Nubp1&Nubp2 knockdown cause a phenotype strikingly similar to that obtained for KIFC5A, namely significant increases in the average number per cell of duplicated centrosomes in mitosis and interphase, and in the number of multi-nucleated cells. Although not providing direct mechanistic evidence, these similar phenotypes, the interactions of Nubp1 and Nubp2 with KIFC5A and between them, and the localisation of KIFC5A and Nubp2 in centrosomes in mitosis, could suggest that two or all three proteins participate in a common pathway involved in the regulation of the cycle of centrosome replication. Understanding the permutations of interactions between the three proteins, the specific role of Nubp2 (as our experiments might suggest a modulatory effect of Nubp2 with an effect in cytokinesis) and finally the targets of these protein complexes will be the focus of our continued studies to enhance our understanding of novel aspects of centrosome duplication.

Materials and Methods

Cell line

Mouse NIH 3T3 fibroblasts were cultured in DMEM containing 10% fetal calf serum (Gibco/BRL), 2 mM glutamine and 50 U/ml of penicillin/streptomycin and maintained at 37°C in 5% CO_2.

Oligonucleotides

All sequences are available as supplementary material (Table S10, supplementary material).

Antibodies

Rabbit polyclonal antibodies to synthetic peptides KGQGGECEIRRASPGSEELT [amino acid (aa) residues 437-456 in mouse KIFC5A (Fig. 1A)] and LTRSLEEGRDFIQEFP [aa 236-251 in mouse Nubp2 (Fig. 7A)] were generated commercially (Sigma-Genosys). They were affinity purified, their specificity characterised by western blotting (Fig. 1C, Fig. 7D) and used at 1:400 dilution for western blotting, 1:300 for immunofluorescence with anti-KIFC5A and 1:30 for all applications with anti-Nubp2. The following other antibodies were used: anti-α-tubulin mouse monoclonal antibody (mAb) (Sigma; 1:4000); affinity-purified rabbit anti-α-tubulin (from the lab of I.V.; 1:100); rabbit anti-γ-tubulin (Santa Cruz; 1:200); affinity-purified mouse mAb anti-myc epitope 9E10 (Santa Cruz; 1:800); mouse anti-dynein (Santa Cruz; 1:600); rabbit anti-pericentrin (a gift from T. Nilsson, University of Goteborg, Sweden; 1:250); anti-centrin mouse mAb (20H5; a gift from J. L. Salisbury, Mayo Foundation; 1:2000); FITC anti-rabbit IgG, Cy5 anti-rabbit IgG, Alexa Fluor 350 anti-rabbit IgG, Alexa Fluor 488 anti-rabbit IgG, Alexa Fluor 488 anti-mouse IgG, Texas Red (TX) anti-rabbit IgG, TX anti-mouse IgG, Alexa Fluor 568 anti-rabbit Ig, Alexa Fluor 568 anti-mouse IgG1 and AMCA anti-mouse IgG.

RT-PCR, semi-quantitative RT-PCR and real time RT-PCR

For RT-PCR, poly(A)$^+$ RNA was extracted from mouse tissues with the RNAeasy purification kit (Qiagen) and 1 μg used for reverse transcription using the Protoscript Reverse Transcription Kit with a $dT_{23}VN$ primer (New England Biolabs).

For the relative quantification of specific RNAs, following siRNA-mediated knockdown, real-time RT-PCR was employed, using the LightCycler system with FastStart DNA Master SYBR Green I reagents (Roche), and specific primers for KIFC5A (oligo set 2), Nubp1 (set 8), Nubp2 (set 9), Eg5 (set 7) and *PBGD* (set 6) (Table S10, supplementary material). *PBGD* served as a normalising gene to equalise for differences in initial RNA amounts between samples.

siRNA-mediated silencing

Catalogue and custom-made Stealth™ siRNA duplexes (Invitrogen) were used for siRNA-mediated silencing: 'MED GC' (medium GC content control silencing oligo); siRNA duplex for KIFC5A, ccgagucucugaauucacuacgcuu/aagcguagugaauucagagacucgg; siRNA duplex for Nubp1, ccacagcagccuacagaaguauaau/auuauacuucuguaggcugcugugg; and siRNA duplex for Nubp2, gguaacuuuacagaacucugcuauu/aauagcagaguucuguaaaguuacc. Transfections with siRNAs were performed on NIH 3T3 cells (30-40% confluency) using Lipofectamine 2000 (Invitrogen) at 1:500 (v/v). Custom-made Stealth siRNA duplexes were used at 40 nM. Transfections were repeated 72 hours after initial treatment. At 120 hours, coverslips were harvested for RNA analysis and microscopic imaging. For monastrol treatment, monastrol was added at 100 μM at 80 hours, washed out 16 hours later, 24 hours before sampling at 120 hours. For each treatment, mitotic cells were scored for the number of centrosomes, as determined by γ-tubulin or centrin staining, spindle morphology (α-tubulin staining) and the count of nuclei per cell. The average and standard deviation (s.d.) of at least three independent counting experiments were determined for test and control treatments. Statistical significance values were assessed by single- or multi-factor ANOVA with replication, as appropriate.

Plasmid vectors

The full-length ORF of KIFC5A, amplified from mouse E13 hippocampal cDNA with oligo set 1, was transferred as a *Bam*HI fragment into mammalian transfection vector pEYFP-C1 (BD Biosciences) to generate YFP-KIFC5A. To construct the myc-tagged version of KIFC5A, vector pSVmyc1.0 was used (Santama et al., 1998) to generate an in-frame *Bam*HI fusion. The truncated KIFC5A-s, amplified from mouse E13 hippocampal cDNA with oligo set 2, was transferred as a *Bam*HI fragment into bacterial expression vector $pHAT_2$ (Peränen et al., 1996) and from there as an *Eco*RI fragment into yeast vector pAS2.1 (Clontech).

The full-length ORF of Nubp1, amplified from NIH 3T3 with oligo set 8, was initially transferred as an *Xho*I fragment into bacterial vector pCR2.1 (Invitrogen) or mammalian transfection vector pEGFP-C3 (BD Biosciences). From pCR2.1, it was subcloned in-frame as an *Eco*RI fragment in yeast vector $pACT_2$ (Clontech).

The cDNA of Nubp2, amplified from NIH 3T3 with oligo set 9, was initially transferred by T/A cloning into bacterial vector pCR2.1 (Invitrogen) and then subcloned as an *Eco*RI fragment into mammalian transfection vector pEGFP-N2 (BD Biosciences) and yeast vector pAS2.1 (Clontech). Nubp2 cDNA, amplified with oligo set 10 and transferred by T/A cloning into pCR2.1, was subcloned as a *Bam*HI/*Xho*I fragment into bacterial vector pGEX-4T-1 (Amersham Biosciences) for expression of GST-tagged Nubp2 and to mammalian vector pSVmyc1.0 (Santama et al., 1998) for expression in NIH 3T3.

Bacterial expression and purification of His_6-KIFC5A-s

For expression and purification of His-tagged KIFC5A-s, competent codon plus DE3 RIL strain of *E. coli* were transformed with $pHAT_2$-KIFC5A-s and single-colony cultures, grown in LB containing 50 μg/ml ampicillin, 30 μg/ml chloramphenicol and 30 μg/ml tetracyclin were used to inoculate 1 L cultures. Large cultures were induced with 0.2 mM IPTG at 20°C overnight. The bacterial pellet was resuspended in 15 ml lysis buffer [20 mM Tris-HCl, 300 mM KCl, pH 7.4, 10% glycerol, 5 mM imidazole and 1 tablet/50 ml of Complete™ (a protease inhibitor cocktail by Roche)], lysed by ultrasonication and centrifuged at 16,000 ***g*** for 30 minutes at 4°C. The soluble fraction was mixed with 40 μl pre-equilibrated Ni^{2+}-NTA beads (Qiagen) and incubated for 30 minutes at room temperature. Beads were washed three times with 10 bead volumes of wash buffer (50 mM Hepes, 100 mM KCl, pH 7.5, 10% glycerol, 10 mM imidazole and Complete) and eluted with 50 mM Hepes, 100 mM KCl, pH 7.5, 10% glycerol, 1 mM $MgCl_2$, 1 mM EGTA, 0.1% β-mercaptoethanol, 250 mM imidazole and Complete.

For ATPase assays, the eluted protein was dialysed against 50 mM Hepes, 50 mM KCl, pH 7.5, 20% glycerol, 1 mM EGTA, 10 mM β-mercaptoethanol and Complete.

For expression of GST-tagged Nubp2 from plasmid pGEX-4T-1-Nubp2, equivalent culture and induction conditions as above were used. Lysis buffer consisted of 20 mM Tris-HCl, 300 mM KCl, pH 7.4, 1% Tween-20, 1 mM β-mercaptoethanol and Complete. The soluble fraction was mixed with 10 μl pre-equilibrated glutathione-Sepharose beads (Amersham Biosciences), washed three times and bound GST-Nubp2 was used for in vitro co-selection experiments.

MT preparation

Tubulin was purified from bovine brain using the procedure of Berliner et al. (Berliner et al., 1994). For motility assays, Rhodamine-labelled MTs were generated as described by Hyman et al. (Hyman et al., 1991) and polarity-marked MTs were

made as per Hyman (Hyman, 1991). For ATPase assays, 5 mg/ml tubulin was polymerised for 30 minutes at 37°C in BRB80 in the presence of 1 mM GTP and 0.3% (w/v) glycerol. Taxol was added at 40 μM and polymerisation continued at 37°C for another 20 minutes. MTs were centrifuged for 30 minutes at 200,000 ***g*** at 30°C and resuspended in 10 mM imidazole, pH 6.8, 5 mM CH_3COOK, 2 mM EGTA, 4 mM $(CH_3COO)_2Mg$ and 20 μM taxol.

ATPase assays

The ATPase activity of KIFC5A-s was assayed in the presence of an ATP-regenerating system as described by Huang and Hackney (Huang and Hackney, 1993). MTs were added at 4 μM and His_6-KIFC5A-s at 0.036 μM. The ATPase reaction was monitored by measuring absorbance at 340 nm.

Motility assays

An anti-His tag antibody (Qiagen) was dissolved at 0.1 mg/ml in BRB80 and incubated for 10 minutes with 0.0375 mg/ml His_6-KIFC5A-s. A 10 μl glass chamber was washed with BRB80, incubated with the motor-antibody mix for 2 minutes and filled with Rhodamine-labelled or polarity-marked MTs in BRB80, including 1 mM ATP and an oxygen-scavenging system (0.06 mg/ml catalase, 0.2 mg/ml glucose oxidase, 20 mM glucose). Fluorescence microscopy was performed using a 60×, 1.4 NA objective lens (Olympus). Images were recorded at intervals of 30 seconds. TILL VISION v.4.01 (TILL PHOTONICS GmbH) was used for generating movies.

Yeast two-hybrid screen

The Matchmaker™, GAL4-based, yeast two-hybrid system (Clontech) was used in conjuction with a mouse embryonic brain cDNA library, constructed in the DNA-activation-domain-bearing $pACT_2$ vector (Clontech). The cDNA of KIFC5A-s was cloned as an *Eco*RI fragment into DNA-binding domain fusion vector pAS2.1 and used as bait. Positive clones were validated after yeast mating with auxotrophy and β-galactosidase assays and identified by DNA sequencing (MWG Biotech). Details about interaction tests for KIFC5A, Nubp1 and Nubp2 are given as supplementary material (Fig. S1, supplementary material).

In vitro co-selection experiments

Co-selection experiments were conducted to confirm the interactions between KIFC5A&Nubp2, KIFC5A&Nubp1 and Nubp1&Nubp2. His_6-tagged KIFC5A-s (the fragment originally used as bait in the yeast two-hybrid screen) was bacterially expressed and bound to Ni^{2+}-NTA beads. GST-Nubp2 was also expressed in *E. coli* and bound to glutathione-Sepharose beads. Nubp1 and Nubp2 were expressed as GFP fusions in NIH 3T3 fibroblasts. Two 60 mm dishes of transfected NIH 3T3 were extracted in a total volume of 1 ml TBS containing 0.05% Triton X-100, 0.05% NP40 and 2 tablets/50 ml of Complete. The extract was mixed with 20 μl of KIFC5A-s-bearing agarose beads or 10 μl of GST-Nubp2-bearing glutathione-Sepharose beads, accordingly, and incubated overnight at 4°C. Negative controls included parallel reactions of GFP vector in conjuction with pre-bound proteins (negative controls) or pre-treated beads without pre-bound proteins incubated with GFP-Nubp2 or GFP-Nubp1, accordingly (additional negative controls). Beads with bound complexes were collected at 400 ***g*** for 5 minutes, washed three times with 10× bed volumes of TBS with 0.05% NP40, re-suspended in SDS sample buffer and boiled. Each sample was split in two, subjected in parallel to two SDS-PAGE runs and western blotting, followed by detection of bound proteins with the appropriate antibodies.

Other molecular biology and protein analysis techniques

Standard molecular biology techniques were performed according to Sambrook et al. (Sambrook et al., 1989). SDS-PAGE was as per Laemmli (Laemmli, 1970) and western blotting was carried out with the semi-dry method (transfer buffer was 48 mM Tris, 39 mM glycine, 20% methanol, pH 9.2). Visualisation of immunoreactive bands was performed by the enhanced chemiluminescence system (Amersham Pharmacia Biotech).

Transient transfections

Cells were transfected by Ca^{2+}/PO_4 precipitation, as applied in Santama (Santama et al., 1998), or with Lipofectamine 2000 (Invitrogen), according to the manufacturer's specifications. Samples were retrieved for microscopic examination or biochemical analysis 20 hours post-transfection for KIFC5A and 10 hours post-transfection for Nubp1 and Nubp2.

Immunolabelling

Cells on coverslips were fixed with 3.7% paraformaldehyde in PHEM (30 mM Hepes, 65 mM Pipes, pH 6.9, 10 mM EGTA and 2 mM $MgCl_2$) for 10 minutes and permeabilised for 15 minutes with 0.5% Triton X-100 in PHEM. Alternatively, cells were pre-extracted for 5 seconds with 0.5% Triton X-100 before fixation or fixed and/or permeabilised in methanol. All cells were quenched with 50 mM ammonium chloride in PBS for 10 minutes, blocked with 2% BSA, 2% FCS, 0.2% fish skin gelatin in PBS ('blocking mix') for 30 minutes and incubated with primary and then secondary antibodies in PBS, containing 5% blocking mix, for 1 hour. Coverslips were mounted with Mowiol (Merck), containing 100 mg/ml DABCO (Sigma) as an anti-fading agent.

Fluorescence microscopy

Immunofluorescent preparations were analysed on a Zeiss LSM510 Confocal Microscope or a Zeiss Axiovert 200M inverted fluorescence microscope equipped with Zeiss Axiovision 4.2 software. Digital images were recorded and composed using Adobe Photoshop 5.0 and Illustrator 10 for the Macintosh.

We thank T. Nielssen and J. L. Salisbury for their kind gift of antibodies. We are grateful to A. Malekkou and A. Ververis for help with yeast two-hybrid experiments, to V. Adamou for help with Nubp2 localisation and to M. Orford for help with FACS analysis. A.C. was supported in part by an A. G. Leventis Foundation (France) doctoral studentship and a short-term EMBO Fellowship. C.W.L. was supported in part by a postdoctoral fellowship from the Telethon Foundation (Cyprus). N.S. was funded by the American Muscular Dystrophy Association (MDA USA) and in part by RTN Network grant IHP-RTN-99-1 (EU).

References

Amos, L. A., van der Est, F. and Löwe, J. (2004). Structural/functional homology between the bacterial and eukaryotic cytoskeletons. *Curr. Opin. Cell Biol.* 16, 1-8.

Ando, A., Kikuti, Y. Y., Kawata, H., Okamoto, N., Imai, T., Eki, T., Yokoyama, K., Soeda, E., Ikemura, T., Abe, K. et al. (1994). Cloning of a new kinesin-related gene located at the centromeric end of the human MHC region. *Immunogenetics* **39**, 194-200.

Badano, J. l., Teslovich, T. M. and Katsanis, N. (2005). The centrosome in human genetic disease. *Nature Rev. Genet.* **6**, 194-205.

Berliner, E., Mahtani, H. K., Karki, S., Chu, L. F., Cronan, J. E. and Gelles, G. (1994). Microtubule movement by a biotinilated kinesin bound to a streptavidin-coated surface. *J. Biol. Chem.* **269**, 8610-8615.

Compton, D. A. (2000). Spindle assembly in animal cells. *Annu. Rev. Biochem.* **69**, 95-114.

de Bettignies, G. and Johnston, L. H. (2003). The mitotic exit network. *Curr. Biol.* **13**, R301.

de Boer, P. A., Crossley, R. E. and Rothfield, L. I. (1989). A division inhibitor and a topological specificity factor coded by the minicell locus determine proper placement of the division septum in *E. coli*. *Cell* **56**, 641-649.

Delattre, M. and Gönczy, P. (2004). The arithmetic of centrosome biogenesis. *J. Cell Sci.* **117**, 1619-1629.

Di Fiore, B., Ciciarello, M., Mangiacasale, R., Palena, A., Tassin, A.-M., Cundari, E. and Lavia, P. (2003). Mammalian RanBP1 regulates centrosome cohesion during mitosis. *J. Cell Sci.* **116**, 3399-3411.

Gaglio, T., Saredi, A., Bingham, J. B., Hasbani, M. J., Gill, S. R., Schroer, T. A. and Compton, D. A. (1996). Opposing motor activities are required for the organisation of the mammalian mitotic spindle. *J. Cell Biol.* **135**, 399-414.

Garrett, S., Auer, K., Compton, D. A. and Kapoor, T. M. (2002). hTPX2 is required for normal spindle morphology and centrosome integrity during vertebrate cell division. *Curr. Biol.* **12**, 2055-2059.

Goshima, G. and Vale, R. D. (2003). The roles of microtubule-based motor proteins in mitosis: comprehensive RNAi analysis in the *Drosophila* S2 line. *J. Cell Biol.* **162**, 1003-1016.

Huang, T. G. and Hackney, D. D. (1993). *Drosophila* kinesin minimal motor domain expressed in *E. coli*: purification and kinetic characterization. *J. Biol. Chem.* **269**, 16493-16501.

Hyman, A. A. (1991). Preparation of marked microtubules for the assay of the polarity of microtubule-based motors by fluorescence. *J. Cell Sci. Suppl.* **14**, 125-127.

Hyman, A., Drechsel, D., Kellogg, D., Salser, S., Sawin, K., Steffen, P., Wordeman, L. and Mitchison, T. J. (1991). Preparation of modified tubulins. *Methods Enzymol.* **196**, 478-485.

Inoue, Y. H., do Carmo Avides, M., Shiraki, M., Deak, P., Yamagushi, M., Nishimoto, Y., Matsukage, A. and Glover, D. M. (2000). Orbit, a novel microtubule-associated protein essential for mitosis in *Drosophila melanogaster*. *J. Cell Biol.* **149**, 153-166.

Kapoor, T. M., Mayer, T. U., Coughlin, M. L. and Mitchison, T. J. (2000). Probing spindle assembly mechanisms with monastrol, a small molecule inhibitor of the mitotic kinesin Eg5. *J. Cell Biol.* **150**, 975-988.

Karabay, A. and Walker, R. A. (1999). Identification of microtubule binding sites in the Ncd tail domain. *Biochemistry* **38**, 1838-1849.

Karsenti, E. and Vernos, I. (2001). The mitotic spindle: a self-made machine. *Science* **294**, 453-547.

Koonin, E. V. (1993). A superfamily of ATPases with diverse functions containing either classical or deviant ATP-binding motif. *J. Mol. Biol.* **229**, 1165-1674.

Kuriyama, R., Kofron, M., Essner, R., Kato, T., Dragas-Granoic, S., Omoto, C. and Khodjakov, A. (1995). Characterization of a minus end-directed kinesin-like motor protein from cultured mammalian cells. *J. Cell Biol.* **129**, 1049-1059.

La Terra, S., English, C. N., Hergert, P., McEwen, B. F., Sluder, G. and Khodjakov, A. (2005). The de novo centriole assembly pathway in HeLa cells: cell cycle progression and centriole assembly/maturation. *J. Cell Biol.* **168**, 713-722.

Laemmli, U. K. (1970). Cleavage of structural proteins during the assembly of the head of bacteriophage T4. *Nature* **227**, 680-685.
Lawrence, C. J., Dawe. R. K., Christie, K. R., Cleveland, D. W., Dawson, S. C., Endow, S. A., Goldstein, L. S. B., Goodson, H. V., Hirokawa, N., Howard, J. et al. (2004). A standardised kinesin nomenclature. *J. Cell Biol.* **167**, 19-22.
Lemos, C. L., Sampaio, P., Maiato, H., Costa, M., Omel'yanchuk, L. V., Liberal. V. and Sunkel, C. E. (2000). Mast, a conserved microtubule-associated protein required for bipolar mitotic spindle organisation. *EMBO J.* **19**, 3668-3682.
Lupas, A., Van Dyke, M. and Stock, J. (1991). Predicting coiled coils from protein sequences. *Science* **252**, 1162-1164.
Maiato, H., Sampaio, P., Lemos, C. L., Findlay, J., Carmena, M., Earnshaw, W. C. and Sunkel, C. E. (2002). MAST/Orbit has a role in microtubule-kinetochore attachment and is essential for chromosome alignment and maintenance of spindle bipolarity. *J. Cell Biol.* **1157**, 749-760.
Matuliene, J., Essner, R., Ryu, J., Hamaguchi, Y., Baas, P. W., Haraguchi, T., Hiraoka, Y. and Kuriyama, R. (1999). Function of a minus-end-directed kinesin-like motor protein in mammalian cells. *J. Cell Sci.* **112**, 4041-4050.
McDonald, H. B., Steward, R. J. and Goldstein, L. S. (1990). The kinesin-like Ncd protein from *Drosophila* is a minus-end directed motor molecule. *Cell* **63**, 1159-1165.
Mitchison, T. J., Maddox, P., Gaetz, J., Groen, A., Shirasu, M., Desai, A., Salmon, E. D. and Kapoor, T. M. (2005). Roles of polymerisation dynamics, opposed motors, and a tensile element in governing the length of *Xenopus* extract meiotic spindles. *Mol. Biol. Cell* **16**, 3064-3076.
Miyamoto, D. T., Perlman, Z. E., Burbank, K. S., Groen, A. C. and Mitchison, T. J. (2004). The kinesin Eg5 drives poleward microtubule flux in *Xenopus* laevis egg extract spindles. *J. Cell Biol.* **167**, 813-818.
Mountain, V., Simerly, C., Howard, L., Ando, A., Schatten, G. and Compton, D. A. (1999). The kinesin-related protein, HSET, opposes the activity of Eg5 and cross-links microtubules in the mammalian mitotic spindle. *J. Cell Biol.* **147**, 351-366.
Nakashima, H., Grahovac, M. J., Mazzarella, R., Fujiwara, H., Kitchen, J. R., Threat, T. A. and Ko, M. S. (1999). Two novel mouse genes-Nubp2, mapped to the t-complex on chromosome 17, and Nubp1, mapped to chromosome 16-establish a new gene family of nucleotide-binding proteins in eukaryotes. *Genomics* **60**, 152-160.
Navolanic, P. M. and Sperry, A. O. (2000). Identification of isoforms of a mitotic motor in mammalian spermatogenesis. *Biol. Reprod.* **62**, 1360-1369.
Nigg, E. A. (2002). Centrosome aberrations: cause or consequence of cancer progression? *Nat. Rev. Cancer* **2**, 815-825.
Ou, Y. and Rattner, J. B. (2004). The centrosome in higher organisms: structure, composition and duplication. *Int. Rev. Cytol.* **238**, 119-182.
Ovechkina, Y. and Wordeman, L. (2003). Unconventional motoring: an overview of the KinC and KinI kinesins. *Traffic* **4**, 367-375.
Peränen, J., Rikkonen, M., Hyvönen, M. and Kääriäinen, L. (1996). T7 vectors with a modified T7*lac* promoter for expression of proteins in *Escherichia coli*. *Anal. Biochem.* **236**, 371-373.
Piel, M., Nordberg, J., Euteneuer, U. and Bornens, M. (2001). Centrosome-dependent exit of cytokinesis in animal cells. *Science* **291**, 1550-1553.
Raskin, D. and de Boer, P. (1999). Rapid pole-to-pole oscillation of a protein required for directing division to the middle of *E. coli*. *Proc. Natl. Acad. Sci. USA* **96**, 4971-4976.
Rost, B. and Liu, J. (2003). The PredictProtein server. *Nucleic Acids Res.* **31**, 3300-3304.
Sakai, N., Yao, M., Itou, H., Watanabe, N., Yumoto, F., Tanokura, M. and Tanaka, I. (2001). The three-dimensional structure of septum site-determining protein MinD from *Pyrococcus horikoshii* OT3 in complex with Mg-ADP. *Structure* **9**, 817-826.
Sambrook, J., Fritsch, E. F. and Maniatis, T. (1989). *Molecular Cloning: A Laboratory Manual.* Cold Spring Harbor, NY: Cold Spring Harbor Press.
Santama, N. (2001). RT-PCR for the identification of developmentally-regulated novel members of the kinesin-like superfamily. In *Neurotransmitter and Neuroreceptor Methods (Methods in Molecular Biology 164)* (ed. I. Vernos), pp. 9-20. New York: Humana Press.
Santama, N., Krijnse-Locker, J., Griffiths, G., Noda, Y., Hirokawa, N. and Dotti, C. G. (1998). KIF2β, a new kinesin superfamily protein, is associated with lysosomes and may be implicated in their centrifugal translocation. *EMBO J.* **17**, 5855-5867.
Saunders, W. (2005). Centrosomal amplification and spindle multipolarity in cancer cells. *Semin. Cancer Biol.* **15**, 25-32.
Saunders, W. and Hoyt, M. A. (1992). Kinesin-related proteins required for structural integrity of the mitotic spindle. *Cell* **70**, 451-458.
Saunders, W., Lengyel, V. and Hoyt, M. A. (1997). Mitotic spindle function in *S. cerevisiae* requires a balance between different types of kinesin-related motors. *Mol. Biol. Cell* **8**, 1025-1033.
Sharp, D. J., Yu, K. R., Sisson, J. C., Sullivan, W. and Scholey, J. M. (1999). Antagonistic microtubule-sliding motors position mitotic centrosomes in *Drosophila* early embryos. *Nat. Cell Biol.* **1**, 51-54.
Shih, Y.-L., Trung. L. and Rothfield, L. (2003). Division site selection in *E. coli* involves dynamic redistribution of Min proteins within coiled structures that extend between the two cell poles. *Proc. Natl. Acad. Sci. USA* **100**, 7865-7870.
Sluder, G. and Nordberg, J. J. (2004). The good, the bad and the ugly: the practical consequences of centrosome amplification. *Curr. Opin. Cell Biol.* **16**, 49-54.
Sluder, G., Thomson, E. A., Miller, F. J., Hayes, J. and Rieder, C. L. (1997). The checkpoint control for anaphase onset does not monitor excess numbers of spindle poles or bipolar spindle symmetry. *J. Cell Sci.* **110**, 421-429.
Walczak, C. E., Verma, S. and Mitchison, T. J. (1997). XCTK2: a kinesin-related protein that promotes mitotic spindle assembly in *Xenopus laevis* egg extracts. *J. Cell Biol.* **136**, 859-870.
Walker, J. E., Saraste, M., Runswick, M. J. and Gay, N. J. (1982). Distantly related sequences in the α- and β-subunits of ATP synthase, myosin, kinases and other ATP-requiring enzymes and a common nucleotide binding fold. *EMBO J.* **1**, 945-951.
Walker, R. A., Salmon, E. D. and Endow, S. A. (1990). The *Drosophila* claret segregation protein is a minus-end directed motor molecule. *Nature* **347**, 780-782.
Zhang, Y. and Sperry, A. O. (2004). Comparative analysis of two C-terminal kinesin motor proteins: KIFC1 and KIFC5A. *Cell Motil. Cytoskeleton* **58**, 213-230.

Journal of Cell Science